Biomaterials Science

ROYAL SOCIETY OF CHEMISTRY

PAPER

View Article Online
View Journal | View Issue

Cite this: *Biomater. Sci.*, 2025, **13**, 4412

The regenerative capacity of cell imprinting and collagen/PCL scaffolds in gastrocnemius tendon defect†

Seyed Aliakbar Hosseini Toopghara,[a] Shahin Bonakdar,*[b] Sara Nayyeri,[b] Morteza Mehrjoo,[b] Fatemeh Ale Ebrahim,[b] Hossein Aminianfar,[c] Farzad Mohammadian Sabour,[c] Leila Montazeri,[d] Mohammad Amin Hajari,[d] Mohammad Ali Shokrgozar,[b] Sang-Won Park*[e,f] and Mohammad Mehdi Dehghan*[c]

Traumatic tendon injuries are among the most common types of injuries, often characterized by insufficient and slow recovery. The current study aims to evaluate the regenerative capacity of a tissue-engineered tendon graft in a rabbit gastrocnemius tendon defect. This graft comprises gap-electrospun collagen-coated parallel polycaprolactone (PCL) fibers seeded with adipose-derived stem cells (ADSCs), which promoted to adopt a tenogenic phenotype using a tenocyte-imprinted substrate for the first time. Scanning electron microscopy (SEM) images confirmed the parallel structure and successful cell attachment to the scaffold. Sirius red staining, high-performance X-ray photoelectron spectroscopy, and water contact angle showed that collagen successfully coated and changed the surface hydrophilicity of the scaffold. Imprinted substrates showed tenocyte patterns in SEM images. In an *in vitro* evaluation, ICC and real-time polymerase chain reaction confirmed that the stem cells acquired tenogenic traits. In addition, histopathology scoring outcomes showed significant improvement in the Pattern group and an almost 2.58 times increase in the total score average compared to the control group. *In vitro* and *in vivo* therapy results show that differentiated ADSCs seeded on the collagen-coated PCL scaffold for tendon repair have astounding therapeutic potential.

Received 9th April 2025,
Accepted 18th June 2025

DOI: 10.1039/d5bm00534e

rsc.li/biomaterials-science

Introduction

Tendon tissue is composed of dense connective tissue that transmits muscle contraction to the skeleton. With aging, tendon injuries become more common.[1] However, tendon tissue lacks the ability of self-renewal and self-recovery. The self-regeneration capacity of the tendon is typically confined to its low vascularity and cellularity.[2] Tenocytes are fully differentiated cells recognized as primary cells with low metabolic activity.[3] Moreover, immune response, infection risks, and limited donor sites are crucial barriers to allograft and autograft transplantation.

Tissue-engineered products represent promising solutions to address challenges for achieving effective healing by utilizing cells, scaffolds, and growth factors. Given the increased risks of side effects associated with growth factors, our focus shifted to utilizing cells and scaffolds. Adipose-derived stem cells (ADSCs) are a suitable cell source because they are abundant and considered an optimal source for obtaining stem cells owing to the simplicity of the isolation process and its low invasiveness.[4] Obtaining ADSCs from the adipose tissue residues of esthetic surgeries eliminates the ethical issues involved when deriving them from bone marrow.[5,6] For the scaffold, we aimed to mimic the natural extracellular matrix of the tissue.

Electrospinning is a primary method for producing low-cost, multifunctional scaffolds for tissue engineering, affording microsized and nanosized scaffolds that imitate the

[a]*Department of Medical Engineering Joint Research, Chonnam National University, Gwangju 61186, Republic of Korea*
[b]*National Cell Bank Department, Pasteur Institute of Iran, Tehran, P.O. Box 1316943551, Iran. E-mail: shahinbonakdar@yahoo.com*
[c]*Faculty of Veterinary Medicine, University of Tehran, P.O. Box 1419963111, Iran. E-mail: mdehghan@ut.ac.ir*
[d]*Department of Stem Cells and Developmental Biology, Cell Science Research Center, Royan Institute for Stem Cell Biology and Technology, ACECR, Tehran, Iran*
[e]*Department of Prosthodontics, School of Dentistry, Chonnam National University, Gwangju 61186, Republic of Korea. E-mail: psw320@chonnam.ac.kr*
[f]*Biomedical Evaluation and Research Centre, School of Dentistry, Chonnam National University, Gwangju 61186, Republic of Korea*
†Electronic supplementary information (ESI) available. See DOI: https://doi.org/10.1039/d5bm00534e

extracellular matrix (ECM).[7] The size and structural resemblance of electrospun nanofibers to ECM makes them ideal for tissue regeneration.[8,9] Significantly, the nanotopographical characteristics exhibited by electrospun nanofibers influence the morphology, migration, and differentiation. The short diameter, adequate contact surface area, and high porosity of electrospun nanofibers have established electrospinning as a frequently employed fabrication method for tissue engineering scaffolds, particularly in wound healing and cartilage, tendon, and nerve tissue regeneration.[10] However, conventional electrospinning does not replicate the organization found in tendon fibers. To address this limitation, gap electrospinning, which can produce uniaxially parallel fibers by manipulating the electric field across the electrode poles, has been developed. Another technique for obtaining aligned nanofibers involves the use of the rapidly rotating-mandrel technique, which is energy- and time-consuming. Moreover, transferring fibers fabricated *via* this method is difficult because they stick to the collecting surface. In contrast, uniaxially aligned nanofibers prepared by gap electrospinning rest on an air gap between the poles, which facilitates the fiber collection procedure.[11]

Polycaprolactone (PCL) is a biodegradable, nontoxic polymer with good mechanical properties.[12,13] However, its poor hydrophilicity and cytocompatibility are unfavorable for creating a cell-friendly scaffold. Accordingly, the surface modification of the PCL fibers without altering their bulk properties is essential.[14] We immobilize collagen on PCL fibers by aminolysis to enhance its cytocompatibility. Collagen is the main component of the ECM and contributes to 65%–80% of the dry weight of tendon tissue.[15] By adding collagen to the fibers, we further mimic the natural chemistry of the tendon tissue.

The cell-imprinting method has been extensively studied to physically mimic the natural topography of cells and induce stable and efficient differentiation signals in stem cells. Several studies have shown the significance of cultural platform elements, ranging from topography, stiffness, and surface nanopatterns in cell differentiation.[16–23] The ECM maintains the physical, chemical, and mechanical functions of a cell, determining the differentiation path for stem cells.[22,24,25] Previously published reports have revealed that a tenocyte-imprinted substrate stimulates tenogenic signals in rat adipose-derived stem cells *in vitro*.[26,27] In other studies, chondrogenic, osteogenic, myogenic, neurogenic, keratinogenic, and Schwann cell differentiation signals were successfully transmitted to stem cells by the imprinting technique.[27–35] The main advantages of the cell-imprinting method for regulating the cell fate are safety, stability, and time and concentration independence. It is a potential replacement for standard polystyrene tissue culture plates as an effective and safe differentiation mechanism.[27]

Polydimethylsiloxane (PDMS) finds extensive application in the imprinting method because of its facile fabrication, gas permeability, optical transparency, and low chemical reactivity.[36] In contrast to conventional tissue culture plastic (TCP), PDMS is nontoxic, modifiable for physio-mechanical features, easily moldable, has high accuracy at the nanoscale and microscale, and has affordable fabrication costs, making it an optimal substrate.[37] Regarding cellular behavior, PDMS gives a more precise perspective of cellular reaction toward mechanical stimulation,[38] stiffness,[39] stretching,[40] and topography.[27,41–43]

In this study, for the first time, we used white New Zealand rabbit (2–3 kg, male) autologous ADSCs that were induced to undergo tenogenic differentiation by a tenocyte-imprinted substrate and grafted onto an injured tendon using collagen-coated, highly aligned gap-electrospun nanofibers for 24 weeks. We aimed to investigate the efficiency of the combined method for the tenogenic differentiation of stem cells.[44] The results of this study could pave the way for future clinical experiments.

Materials and methods

All animal procedures were performed in accordance with the Guidelines for Care and Use of Laboratory Animals of the University of Tehran and approved by the Animal Ethics Committee of the Faculty of Veterinary Medicine, University of Tehran (Approval ID: IR.UT.VETMED.REC.1403.050).

Scaffold

Fabrication of the PCL scaffold. PCL (average M_n = 80 000, Sigma, USA) was dissolved in a dichloromethane (Merck, Germany) and dimethylformamide (Merck, Germany) mixture (80 : 20) to obtain PCL solution. The solution was allowed to rest for 30 min at room temperature and then stirred as required to form a homogeneous solution. The compound was centrifuged at 2000 rpm for 5 min to eliminate air bubbles. We extruded the solution using a 21G syringe on the collector under 15 kV at a flow rate of 0.75 ml h^{-1}. We designed a collector explicitly for this study, comprising two twin copper sheets aligned horizontally, facing each other with a 3 cm gap.[10] ESI Fig. 1† presents a schematic view of the electrospinning compound.[45]

Fiber diameter and orientation analysis. Three 1 cm × 1 cm parts were cut from the scaffold and coated with gold. Each sample was viewed with a scanning electron microscope (TeScan-Mira3, Czech Republic). Three representative images were taken for each sample, and the diameter and orientation of 175 distinct fibers were measured using ImageJ (NIH, USA). Scanning electron microscopy (SEM) images with 1k magnification were used for fiber diameter measurement. The angle of each fiber was relative to the *x*-axis and was taken as the fiber orientation. Graphs of fiber diameter distribution and fiber orientations were plotted using Origin software (version 2019b).

Collagen coating. Fabricated nanofiber mats were washed by immersion in 50% v/v ethanol solution for 3 h and then rinsed with deionized water to remove oily contamination. The nanofibers were then immersed in a 10% w/v solution of ethylenediamine/2-propanol at 37 °C for 24 h and washed with deionized water for another 24 h. Afterward, they were soaked in 1% w/v glutaraldehyde solution for 3 h at 25 °C, washed with

deionized water three times, and immersed in deionized water for 24 h to expel unreacted glutaraldehyde molecules. Finally, the amine-functionalized nanofiber mats were immersed in a collagen solution (3 mg ml^{-1}, NanoZist Arayeh, Iran, calfskin) with a pH of 3.4 and incubated at 4 °C for 24 h. The collagen-coated fibers were rinsed with 1% acetic acid solution and then rinsed with deionized water for 24 h to remove excess collagen.[14]

Sirius Red staining. Sirius red staining was conducted by utilizing picrosirius red solution and acidic water. Sirius red is a strong anionic dye that stains collagen *via* a reaction between its sulphonic acid groups and the basic groups present in the collagen molecule.[46] Picrosirius red solution was formulated by dissolving 0.5 g of Sirius red dye powder (Sigma) in 500 ml of saturated aqueous picric acid solution. Additionally, acidic water was prepared by mixing acetic acid with deionized water (0.5% v/v). The fabricated mat was initially soaked in the picrosirius red solution for 1 h to reach near equilibrium during staining. Then, it was rinsed thoroughly with the acidic water solution (two times).[47] Samples of uncoated and collagen-coated PCL parallel fibers were observed by polarized light microscopy.

Water contact angle measurement. The contact angle quantifies the scaffold surface wettability. In this test, a low contact angle indicates a more hydrophilic surface. Hydrophilic surfaces could enhance cell attachment of mammalian cells to the scaffold.[48]

High-performance X-ray photoelectron spectroscopy. High-performance X-ray photoelectron spectroscopy (HP-XPS) was performed (K-Alpha+, Thermo Fisher, USA) to confirm the successful surface-modification process. A standard N 1s survey scan was employed to investigate the pristine PCL fibers (PCL), PCL fibers after diamine addition (PCL-DN), and collagen-coated PCL fibers (PCL-Col).[14]

Cell viability and proliferation of the scaffold. To evaluate the cell viability and proliferation of the scaffold, we used the L929 cell line (ACTC, USA). Cells were seeded at 5×10^3 cells per well on the scaffold in 24-well plates and cultured for 1, 3, and 7 days in RPMI medium supplemented with 10% fetal bovine serum (FBS) (Gibco, Switzerland) and 1% antibiotic–antimycotic (100×) (Gibco, Switzerland). The culture medium was replaced with fresh media every 2–3 days. We used normal 24-well plates (SPL, Korea) to culture the positive control group and ultralow attachment plates (SPL, Korea) for the test groups. Cell proliferation and viability were assessed using the water-soluble tetrazolium salt (WST) assay (EZ-CYTOX, Dozen Bio Co, Korea). WST solution was added to each well to prepare a 10% solution and then incubated for 1 h. Afterward, the samples were shaken gently for 1 min. The optical density of the extracted solution was analyzed at an absorbance wavelength of 450 nm in a microplate reader (Synergy H1 Hybrid Multi-Mode Reader, BioTek, USA). The experiment was repeated twice ($n = 6$).[49,50]

Cell attachment and orientation analysis. The third passage of the isolated ADSCs was cultured on the collagen-coated scaffold. Scaffolds were fixed on the plate with sterile stainless-steel needles for stability and cultured in Dulbecco's modified Eagle's medium (DMEM) supplemented with 10% FBS, 1% antibiotic–antimycotic (100×), and 5% CO_2 at 37 °C under humid conditions. After seven days, the seeded scaffold was fixed with 4% w/v glutaraldehyde for 20 min and stained with crystal violet. The images were used to measure the cell orientation of 150 cells in five samples using ImageJ software and graphs plotted with Origin software (ver. 2019b). Cell attachment was determined by SEM imaging. Cells were washed twice with phosphate buffered saline (PBS) after fixation (glutaraldehyde 4%) following dehydration with serial dilution of ethanol (40 – absolute ethanol) for 10 min.[50]

Imprint substrate

Isolation of tenocytes. Isolated tenocytes were used to prepare the imprint substrate, and these cells were not directly used in the final implantation. Rabbits were euthanized according to ethical principles.[51] Gastrocnemius tendon samples of the rabbits were obtained under aseptic conditions. The acquired tendon tissue was washed with 15 ml of PBS, supplemented with 3% antibiotic–antimycotic (100×). Subsequently, the tissue was mechanically minced in a sterile culture plate and treated enzymatically with 0.25% trypsin/EDTA (Sigma, USA) for 30 min. After neutralizing the trypsin with FBS, the samples were incubated in a collagenase type 1 (0.5% w/v, Sigma, USA) solution for 15 h. Lastly, the digested tissue was centrifuged, and cell pellets were collected and cultured in DMEM (Gibco, Switzerland) supplemented with 10% FBS (Gibco, Switzerland), and 1% antibiotic–antimycotic (100×) in six-well culture plates (SPL, Korea).[27]

Development of a cell-imprinted substrate. Confluent tenocytes without any passage were fixed with 4% w/v glutaraldehyde for 24 h following washing with PBS. To remove the residual salts of the PBS in the plates, they were washed gently for 20 s with distilled sterile water and dried at room temperature. Nanoscale patterned substrates were produced by blending one part of the curing agent with 10 parts of a silicone elastomer base (PDMS, Sylgard 184, RTV Dow Corning). The PDMS casting procedure was conducted by pouring the same amount of prepared PDMS solution onto the fixed tenocytes and preserving it at 37 °C for 48 h. The cured PDMS substrates were washed in boiling distilled water for 10 min and then washed with 1 M sodium hydroxide at room temperature for 15 min to remove any cell residuals or proteins. The substrates were sterilized by autoclaving before further use. These substrates were used as cell culture plates for seeding ADSCs.[27,43]

ADSC isolation and differentiation. We surgically extracted adipose tissue from the interscapular region of rabbits. To utilize autologous ADSCs, the cell-isolation process was performed separately for each rabbit. After the surgical procedures, the samples were transferred into 30 ml of PBS supplemented with 3% antibiotic–antimycotic (100×). The adipose tissues were rinsed with PBS to remove as much blood as required. The tissues were then mechanically minced to not less than 2 mm parts, and connective tissues and blood vessels were removed. Then, the adipose tissues were enzy-

matically treated with 0.5% w/v collagenase type I for up to 2 h at 37 °C in a shaking incubator. After removing any undigested tissues from the container, the remaining tissues were centrifuged to obtain cell pellets. After removing the supernatant, the cells were resuspended and cultured in DMEM supplemented with 10% FBS, 1% antibiotic–antimycotic (100×), and 5% CO_2 at 37 °C under humid conditions. After the third passage, these cells were either seeded directly on the scaffold for implantation or seeded on the imprint substrates for 14 days for differentiation and then transferred to the scaffold for implantation. The cells were cultured overnight to attach perfectly to the scaffold prior to implantation.[27,43]

Flow cytometry. The successful isolation of the ADSCs was confirmed by flow cytometry, which was conducted by investigating the genes CD44, CD90, CD34, and CD45 in 1×10^6 cells at their third passage. CD44 and CD90 are surface markers commonly used to identify and characterize mesenchymal stem cells. In contrast, CD34 and CD45 act as negative controls because they are positive markers for hematopoietic stem cells.[52]

Microscopic observation. The surface characteristics and morphological details of the samples were evaluated by employing optical microscopy (Olympus, Japan) and SEM (TeScan-Mira3, Czech Republic).

Expression profiling. Real-time polymerase chain reaction (PCR) was performed to investigate the *in vitro* functional behavior of the differentiated ADSCs compared to that of ADSCs cultured on plain PDMS. A total of 2×10^4 cells were seeded and cultured for 14 days on tenocyte-imprinted substrates (Pattern) and nonpatterned substrates (PDMS). RNA was extracted according to the manufacturer's protocol using Trizol, and DNA content was eliminated using DNase I. Then, using Nanodrop (Thermo Scientific, USA), RNA concentration was evaluated. cDNA was synthesized according to the manufacturer's protocol (PrimeScript RT Master Mix, TAKARA, Kyoto, Japan). Collagen type one (COL1), tenomodulin (TNMD), tenascin (TNC), and scleraxis (SCX)[53] as tenocyte gene markers and GAPDH as an endogenous control were assessed in the experiment. For negative controls of other lineages, aggrecan (AGR) for chondrogenic and RUNX2 for osteogenic were included. The sequence of genes used for evaluation is listed in ESI Table 1.†[26,27,54]

Immunocytochemical staining. ADSCs (2×10^4) were seeded and cultured for 14 days on three nonidentical culture platforms, including cell-imprinted substrates (Pattern), regular culture plate, and nonpatterned substrate (PDMS). Immunocytochemical staining (ICC) of the cells was performed using the anti-tenomodulin antibody (Merck, SAB2102497) as the primary antibody and anti-horseradish peroxidase (HRP) as the secondary antibody. 3,3′-Diaminobenzidine (DAB, Sigma-Aldrich, D7304) was utilized for visualization. The samples were washed twice with PBS and then fixed with 4% w/v paraformaldehyde in PBS for 15 min at room temperature. Then, the fixative was aspirated and the samples were rinsed two times in PBS for 5 min each. Subsequently, the samples were incubated with normal serum block-species, the same as the secondary antibody, for 15 min to block the nonspecific binding of immunoglobulin. Then, the specimens were incubated with the primary antibody in antibody dilution buffer overnight at 4 °C. In this part, the samples were incubated in peroxidase blocking solution for 10 min at room temperature. Then, the cells were incubated by anti-polyvalent HRP polymer detection (EURMAB-Italia) in PBS for 30 min at room temperature. Finally, they were incubated in DAB solution for 3 min. The nuclei of the cells were stained with hematoxylin dye. The samples were dehydrated with 95% v/v ethanol for 2 min and absolute ethanol twice for three minutes, and assessed using an optical microscope (Olympus CX33). Finally, the results were quantified using the IHC Profiler Plugin in ImageJ software.[55]

In vivo examination

Cell seeding on the fabricated scaffold. ADSCs cultured on the tenocyte-imprinted substrate for 14 days were dispersed by trypsinization and seeded on the collagen-coated nanofibers at a population of 8×10^5 cells and then incubated overnight in DMEM supplemented with 10% FBS, 1% antibiotic–antimycotic (100×), and 5% CO_2 at 37 °C under humid conditions to ensure firm cell attachment to the scaffold. Then, the cell-attached scaffold was folded to keep parallel fibers aligned to the receiver tendon fibers. The tendon graft was thus ready to implant into the wounded tendon tissue. For the undifferentiated group (ADSCs), cells were seeded on the scaffold in the third passage.

Tendon injury induction. Anesthesia was induced in rabbits with 50 mg kg^{-1} of ketamine (Alfasan, Netherlands) and 20 mg kg^{-1} of xylazine (Alfasan, Netherlands). To maintain anesthesia, the rabbits were administered isoflurane inhalation. A lateral incision of the fascia and paratenon was made to expose the Achilles tendon. The gastrocnemius tendon was isolated from the soleus and plantaris tendon. A 3 mm circular defect was induced in the gastrocnemius tendon by a biopsy punch when the tendon was not under tension.[56] Subsequently, the rabbits were randomized into four groups (five rabbits for histopathology and one rabbit for mechanical test per group). The first group had left gastrocnemius tendon injury sutured with a 6–0 nylon thread (Supa, Iran) to mark the margins of injured area. This group received no treatment (control group). The second, third, and fourth groups had left gastrocnemius tendon injury implanted with the cell-free scaffold, ADSC-seeded scaffold, and differentiated ADSC-seeded scaffold, respectively. The rabbits received a three-day subcutaneous administration of enrofloxacin (HIPRA, Spain, 5 mg kg^{-1}) and tramadol (Chimie Darou, Iran, 10 mg kg^{-1}). The animals were sacrificed after 24 weeks, and tissue segments were prepared for histological analysis.

Histological evaluation. After harvesting the Achilles tendon of each rabbit, tissue specimens were fixed in neutral buffered 10% w/v formalin for three weeks. Longitudinal sections of the injured and adjacent normal tendons were obtained to prepare paraffin blocks. Tissue sections with a 4 μm thickness were stained with hematoxylin–eosin (H&E) and Masson's trichrome. The slides were evaluated using the semiquantitative

grading system for the following variables:[56] the ECM, cellularity, cell alignment, cell distribution, nucleus morphology, callus configuration and homogeneity, maturation of the callus-to-native tendon interface, inflammation, vascularity, and degenerative changes. The sum of the scores was calculated as the total score for each slide. Histological scores were statistically analyzed using an ordinary one-way analysis of variance (ANOVA) test followed by a Bonferroni test as a multiple comparisons test. This analysis was performed using GraphPad Prism 9.0.0 for Windows software.

Mechanical properties. After 24 weeks, the rabbits were sacrificed humanely, and the gastrocnemius tendon was harvested. The samples were kept in PBS-moist gauze before the test. Then, the samples were fitted into a tensile test machine (Santam, Iran) clamp with a travel speed of 10 mm min^{-1} (n = 1).

Results and discussion

Scaffold

PCL has been studied extensively, and its safety and biocompatibility make it a good candidate for tissue engineering.[57] Furthermore, PCL has superior usability in electrospinning; this function is more critical in the gap version because the fiber orientation is very sensitive to polymer consistency and could directly affect the final results. We found that a 12.5% w/v solution worked better in our setup than 7.5%, 10%, and 15% w/v concentrations (data not included). The viscosities of the 7.5% and 10% w/v solutions were too low, and the bead formation and alignment failure occurred frequently. The effect of viscosity on the bead formation in aligned fibers has been reported previously in electrospinning. Increasing the concentration changes the bead from a spherical to a spindle-like shape until it finally becomes smooth fibers.[58] Conversely, the 15% w/v solution was too thick, and needle blockage occurred frequently; thus, the final product lacked consistency. The 12.5% w/v solution provided the favorable fiber diameter (average 955 nm, Fig. 1A4) close to the natural tendon fibril size, 50–5000 angstroms.[59] We also observed that fresh PCL solution had to be used directly after completely dissolving PCL pellets; otherwise, the fibers failed to orient correctly.

Fig. 1A1 depicts the custom-made receiver part of the gap-electrospinning apparatus. Fibers successfully follow the electric field. The * sign indicates the conductive parts of the receiver (copper plates). The area between the conductive parts depicts the parallel fibers, the part used as the scaffold. The surrounding area shows the fibers that follow the electric field in a semi-circular shape (waste area). Fig. 1A3 and A2 present the SEM images of the low and high densities of the fibers. The fiber orientation angle depicted in Fig. 1A5 is highly parallel. The fiber orientation is closely followed by the ADSCs (Fig. 1C4).

PCL has a hydrophobic nature, which is disruptive to cell adhesion. We aimed to overcome this flaw by coating the scaffold with collagen. The coating boosts cell adhesion and proliferation and mimics the tendon tissue chemistry.[60] PCL is an aliphatic polyester with abundant ester groups (–COO–). Amino groups can be introduced to the surface by a reaction with diamine. One amino group undergoes covalent bonding with a –COO– group, creating –CONH–, while the other amino group remains unreacted and ready to be used. Later, this amino group is utilized to coat collagen.[14]

To confirm the existence of collagen on the fibers, we used Sirius red staining to visualize the existence of the collagen. In the macroscopic view (Fig. 1B1), the collagen-coated scaffold turned red, while the noncoated scaffold did not show color changes (Fig. 1B3). These results were confirmed under the polarized light microscopy of the scaffolds (Fig. 1B2 and B4). The denser color on the margin indicated with * is the area where multiple layers are stacked on each other (Fig. 1B2).

To further confirm the coating, we used HP-XPS to investigate N_{1s} on PCL, PCL-DN, and PCL-Col. The amount of elemental N in the samples was 0%, 0.27%, and 1.8%, respectively (Fig. 1B9), which indicates the existence of NH_2 groups in the successful coating of ethylenediamine and the protein. The HP-XPS analysis revealed the appearance of an N_{1s} peak at 400.2 eV after the immobilization of the collagen, which confirmed the coupling (Fig. 1B8).[14]

Fig. 1C2 depicts the high concentration of the fibers after collagen coating. Interestingly, the wavy structure of the fibers (red lines highlighted the waves) resembles the normal wavy shape in tendon tissue.

We conducted water contact angle analysis to evaluate the competency of the coating technique in overcoming the hydrophilicity of PCL. Fig. 1B5 shows a comparison of the water contact angles immediately after dropping and after stabilization (15 seconds) of random and parallel fibers (Fig. 1B6) compared with those of collagen-coated parallel fibers (Fig. 1B7). The average water contact angle dropped from 60° to 47° upon changing the fiber orientation to parallel. After the collagen coating of parallel fibers, the water drop was absorbed into the scaffold, making a 0° contact angle. These results suggest that the collagen coating significantly affects hydrophilicity, and fiber orientations could also significantly reduce the water contact angle. These results indirectly suggest the successful collagen coating procedure (n = 5).

After successful coating on PCL, the cell culture confirmed the ability of the scaffold to orient the cells. Fig. 1C1 reveals that the cells were well attached to the collagen-coated fibers. Fig. 1C3 depicts the optical microscopy images of ADSC-seeded scaffolds after crystal violet staining. Highly parallel fibers fabricated by the gap-electrospinning technique enabled the cells to follow the aligned fibers, which resembled the natural tendon tissue cell orientations. The cell orientation closely followed the orientation of the fibers (Fig. 1C4). In addition, the homogeneous spreading of the cells over the scaffold indicated consistent collagen coating on them. Moreover, the spindle morphology of the ADSCs was well-preserved on the surface of the scaffold, which mimicked the standard tendon cell composition with adequate similarity.

The WST test for cell viability over 24 h (Fig. 1D1) showed that the collagen-coated PCL parallel fibers (Col-Para PCL) had significantly superior viability compared to collagen-coated

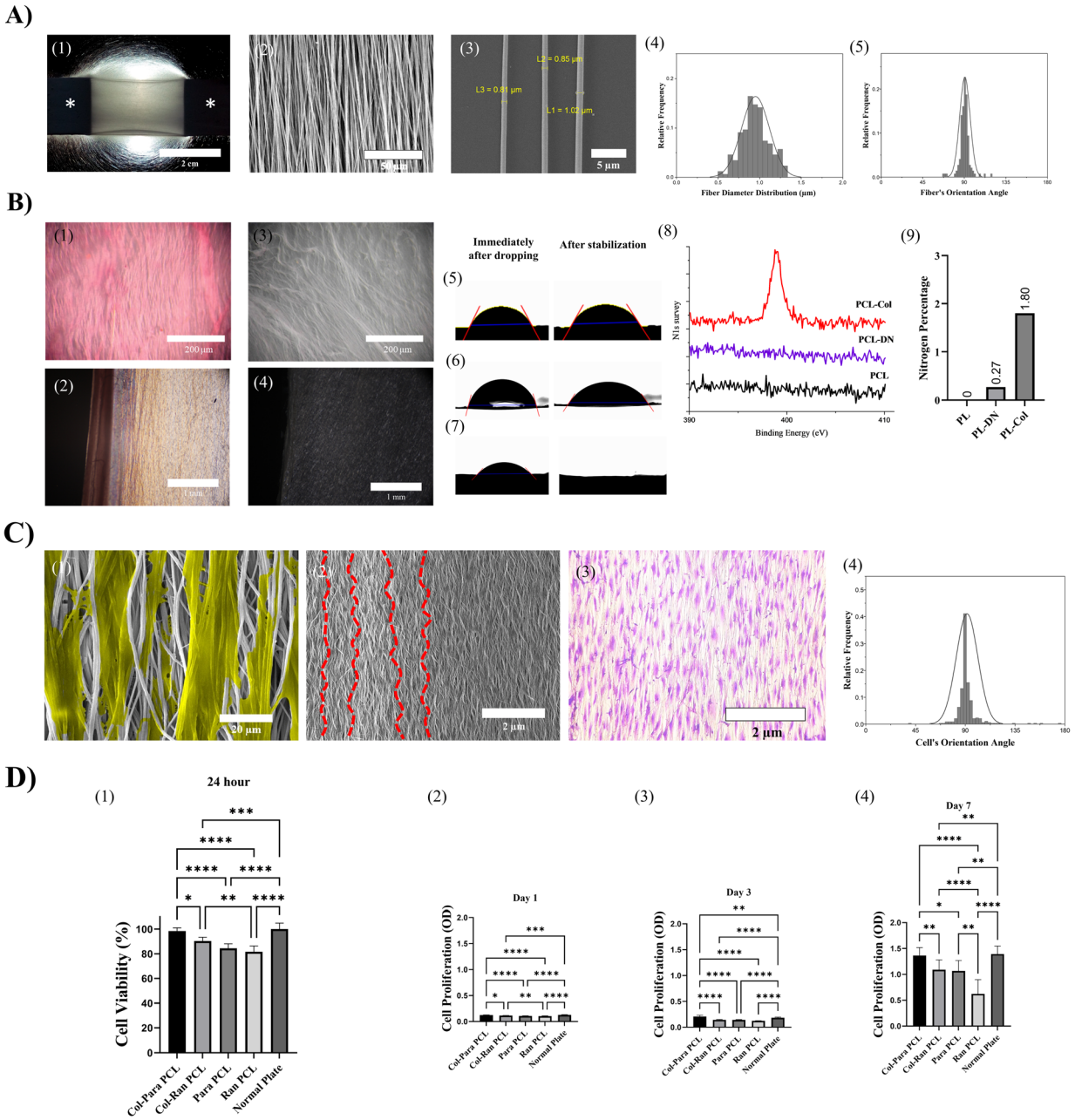

Fig. 1 Fabrication process (A), chemical evaluation (B), and biological evaluation (C) of the scaffold. The actual scaffold on the target side of the electrospinning apparatus. The * indicates the copper sheet parts and the parallel fibers located in the middle (A1). SEM image of the high density of fibers before collagen coating (A2). The SEM image shows the low concentration of the PCL fibers (A3). The graph (A4) depicts the fiber diameter distribution. Fiber orientation angle (A5). Light microscopy of Sirius red staining of the collagen-coated scaffold (B1) and noncoated PCL fibers (B3). Polarized light microscopy of the collagen-coated scaffold (B2) and noncollagen-coated scaffold (B4). Water contact angle of the material surface before (left image) and after stabilization for 15 seconds (right image) on PCL random fibers (B5), parallel fibers (B6), and collagen-coated parallel fibers (B7). Graph showing the N_{1s} survey graph (B8) and the percentage of nitrogen content on PCL scaffolds (B9). In C, we aim to show the cell and fiber orientation and attachment. Yellow pseudo-coloring highlights the cells attached to the scaffold after collagen coating (C1). SEM image of the high density of fibers after collagen coating. The red line shows the wavy shape of fibers (C2). Light microscopy image of the crystal violet staining of cells on the scaffold (C3). Cell orientation angle distribution (C4). Cell viability at 24 h of the culture graph (D1). Cell proliferation on days 1, 3, and 7 (D2–4). (*p < 0.05, **p < 0.01, ***p < 0.001, and ****p < 0.0001).

PCL random fibers (Col-Ran PCL), PCL parallel fibers (Para PCL), and PCL random fibers (Ran PCL). There was no significant difference between TCP plates (normal plate) and the Col Para PCL group. The cell proliferation on days 1, 3, and 7 revealed the significant superiority of the Col-Para PCL compared to other test groups and had no significant differences with normal culture plates (Fig. 1D2–D4). This finding confirms the competency of the PCL surface modification (n = 5).

Imprinting substrates

The cell-imprinting method has been investigated in the *in vitro* stage before; however, the results of the *in vitro* stage were controversial. For example, Haramshahi *et al.* reported promising results regarding the ability of the cell replica to induce tenocyte marker expression in ADSCs *in vitro*. However, in the *in vivo* immunohistochemistry, they observed little difference between untreated ADSCs and ADSCs cultured on tenocyte-imprinted substrates. They used a pooled source of allogeneic ADSCs and implanted it subcutaneously on the median backside of rats. Obviously, some aspects could negatively affect the results, such as the allogeneic cell source, a nonspecific region of implantation, and a short duration of 4 weeks for the slow-healing nature of tendon tissue.[26] In our study, we chose to implant it in the actual target tissue to obtain a more valid result. We used the rabbit as a large animal model to facilitate the implantation accuracy and access the larger area of tendon tissue (compared to rats in the study of Haramshahi *et al.* (2020)[26]). We targeted the gastrocnemius tendon in the Achilles tendon. We used autologous ADSCs for each rabbit and increased the study duration to 24 weeks. With these changes, we consider our results to be more reliable than those reported in previous studies.

ADSC isolation. After extracting adipose tissue from the interscapular region of rabbits (ESI Fig. 2†), we utilized flow cytometry to validate the successful isolation of ADSCs. CD44 and CD90 (Fig. 2a and b) were the standard surface markers used for identifying and characterizing mesenchymal stem cells. Conversely, CD34 and CD45 (Fig. 2c and d) were negative controls due to their association with hematopoietic stem cells. The results showed that 100% of cells expressed CD44 and 98.2% expressed CD90. The negative controls presented 0.411% and 0.278% expression for CD34 and CD45, respectively.

Tenocyte substrates. After the isolation of the tenocytes from the tendon tissue, their expansion and fixation were carried out, as mentioned in the Materials and methods section. In Fig. 2e, the topographical fingerprints of fixed tenocytes are visible on the surface of the fabricated substrate. Before being

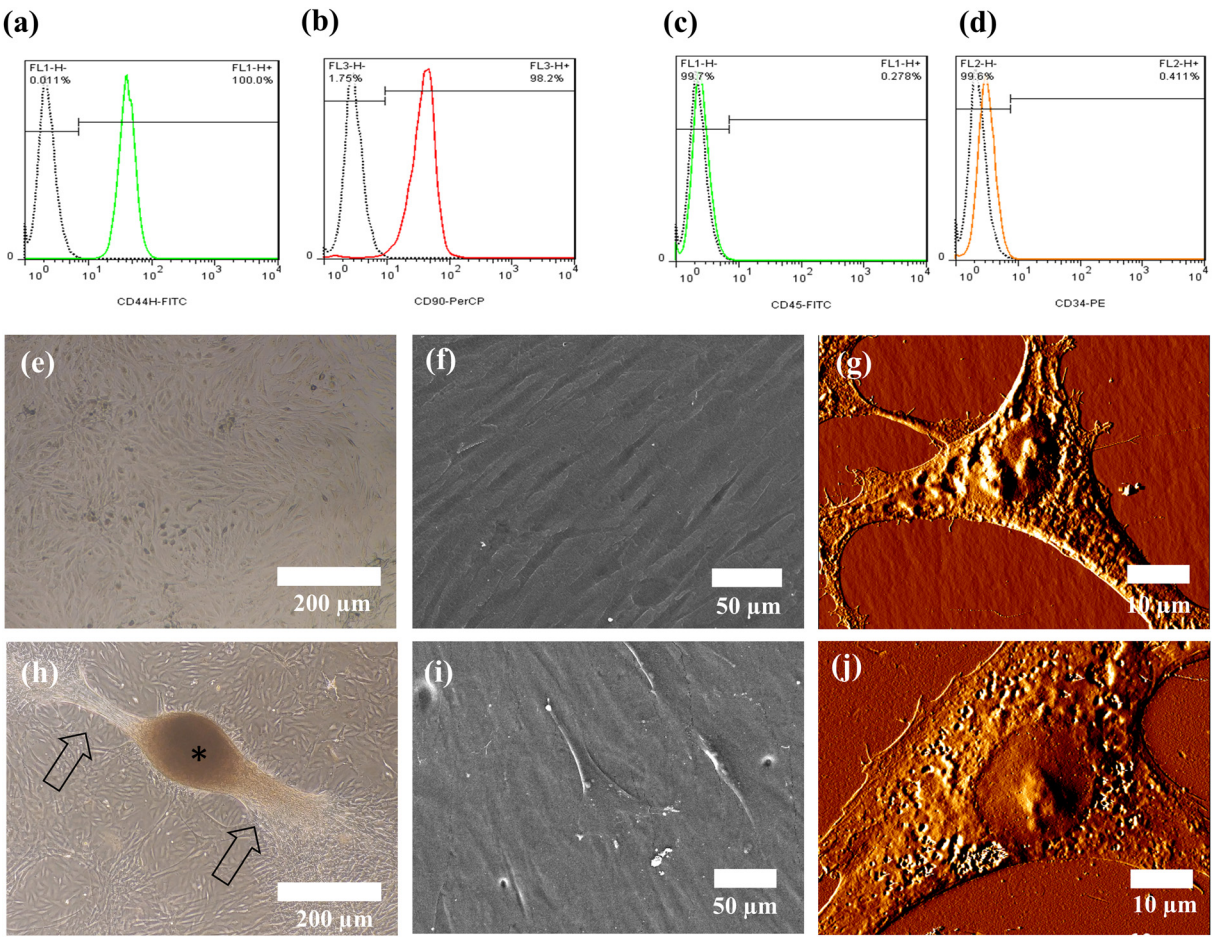

Fig. 2 ADSCs, tenocytes, and imprint substrates. Flow cytometry results of CD44 (a) and CD90 (b) related to the mesenchymal lineage and CD45 (c) and CD34 (d) for the hematopoietic lineage. Light microscopy image of the PDMS cell-imprinted substrate with replicated spindle shapes observable on the surface (e). SEM image of the PDMS imprint substrates (f). AFM image of a tenocyte (g) and ADSC (j). ADSC clusters on the imprint substrate after 14 days. The * sign indicates the cell cluster, and the arrows indicate the tendon-like bundle of the cells in the culture plate (h). Single cells follow the substrate topography (i).

fixed, tenocytes were highly confluent, which yielded fully cell-imprint-covered, consistent culture platforms with almost no bare PDMS surface to come in contact with the ADSCs. Consequently, it provided harmonious results concerning cell differentiation and morphological adaptation. The specimen was washed thoroughly with boiling water and NaOH to eliminate cell residuals and prevent unwanted biochemical interactions with ADSCs. Fig. 2f depicts the SEM image of the surface of the PDMS imprint, which successfully takes up the imprint of the tenocytes. Fig. 2g and j depict the atomic force microscopy (AFM) images of the tenocytes and ADSCs, respectively. Although both tenocytes and ADSCs usually have the same spindle morphology, ADSCs are significantly larger than tenocytes in rabbits. In addition, there are differences in cell topography. Other researchers also indicated that although these cells are quite similar in morphology, they demonstrate nanotopographical differences.[23]

An accidental finding in the current study was the effect of the imprint quality of the PDMS cast on the cells. On the basis of the previous PDMS cast protocol for PDMS imprinting fabrication by the Bonakdar research group, unlimited casting was performed on fixed cells until a visible defect occurred in the fixed cells. In our study, we limited the casting attempts to a maximum of three times. Interestingly, after 14 days of culture on the substrates, this change directly affected the ADSCs. We observed cell clusters in the plates that mostly used the first-time casting of the fixed cells, less frequently on the second, and almost no cluster on the third casting (Fig. 2h). These cell clusters were up to 14.5 times longer than a single tenocyte cell. Arrows at the poles of such a cluster (Fig. 2h) indicate a bundle structure of cells that have a remarkably similar appearance to a tendon structure. The * sign indicates the body of the cell cluster. Because the topographical shapes on the cells are at the nanoscale,[23] multiple casting could negatively affect the fixed cells used as the source of imprints and probably destroy some delicate profiles. As the imprint substrate had been vigorously washed with boiling water and NaOH solution, we assumed that no biological residue remained in the substrates. Although the cell clusters became less frequent by further casting, we still observed the positive effect of the third casting in immunocytochemistry and real-time PCR in this study. However, it can be argued that the results would vary between studies because they did not track how often fixed-source cells were used. Further investigation is needed to make a definitive argument regarding the reasons, which are beyond the scope of this study.

Immunocytochemical staining. To investigate the competence of the cell-imprinted platform for ADSC tenogenic induction further, immunocytochemical staining was performed (Fig. 3). Because of the significance of tenomodulin in the tendon structure,[61] an anti-tenomodulin antibody was selected for this test. First, we attempted fluorescence staining; however, owing to a low expression of tenomodulin in undifferentiated groups and the lack of the ability to visualize it on a macroscopic scale, the comparison lacked the details sought. Thus, chromogenic immunocytochemical staining was performed. Macroscopic visualization depicts distinctive differences between groups. The microscopic view in the IHC profiler and results show a distinctive graph difference between groups (Fig. 3g–i). The pixel counter report of the IHC profiler showed positive results for the Pattern group and negative expression for the Plate and PDMS groups (Fig. 3j–l). The highest level of tenomodulin was detected in ADSCs cultured on a cell-imprinted platform (Pattern), which further suggests that tenocyte topography promotes tenogenic differentiation in ADSCs. The hydrophobic nature of PDMS interferes with cell adhesion, which negatively affects propagation and differentiation, as observed in Fig. 3c and f. Cell imprinting on the PDMS surface enhances cell adhesion (as seen in Fig. 3a and d), likely due to increased surface area availability and surface irregularities that facilitate better cell anchoring.

Gene expression profiling. Fig. 3m presents the contrast between gene expression profiling of undifferentiated ADSCs cultured on nonpatterned substrates (PDMS) and ADSCs cultured on the bioengineered cell-imprinted substrates (Pattern). An increase in the expression of tenocyte genetic markers—tenomodulin (1.85 times), tenascin (1.33 times), and SCX (1.31 times)—was observed in ADSCs treated on imprinted substrates to undergo tenogenic differentiation compared to non-treated ADSCs. Statistical analysis was conducted using two-way ANOVA and Šídák's test as the multiple comparisons test (GraphPad Prism 10.2.3) (n = 4).

In vivo examination

We designed four groups for the *in vivo* examination to evaluate the differentiation method and scaffold capacity for use as a tendon graft. The process started with the isolation of ADSCs from each individual rabbit. The isolated cells were subcultured until the third passage. For the main test group (Pattern), the cells were transferred on tenocyte-imprinted substrates to differentiate for 14 days and then seeded on the scaffold and implanted into the defect area. We used the third passage of the undifferentiated ADSC group (ADSCs) as the control group of the pattern group. To evaluate the mere effect of collagen-coated gap-electrospun parallel fibers, a noncell seeded scaffold was implanted into the defect area (Scaffold). The last group was the overall control group with a defect without a scaffold or cells (Control).

Tendon defect induction and autograft implantation. Fig. 4A1–A4 show the defect induction procedure and autograft implantation steps in the rabbit gastrocnemius tendon. The defect was created using a 3 mm biopsy punch (4A1) at the center of the tendon while it was in a relaxed position. In Fig. 4A2, the tendon is stretched, affecting the defect size and changing the shape temporarily. We ensured that the scaffolds would not tear apart and dislocate if the tendons were stretched. After 24 weeks of treatment, there was a notable variation in the wound area length among the study groups. We chose nylon as a nonabsorbable suture to facilitate easy localization of the defect after 24 weeks. We used this as the defect margin marker even in the control group. In the control group in which no intervention was included, the average dis-

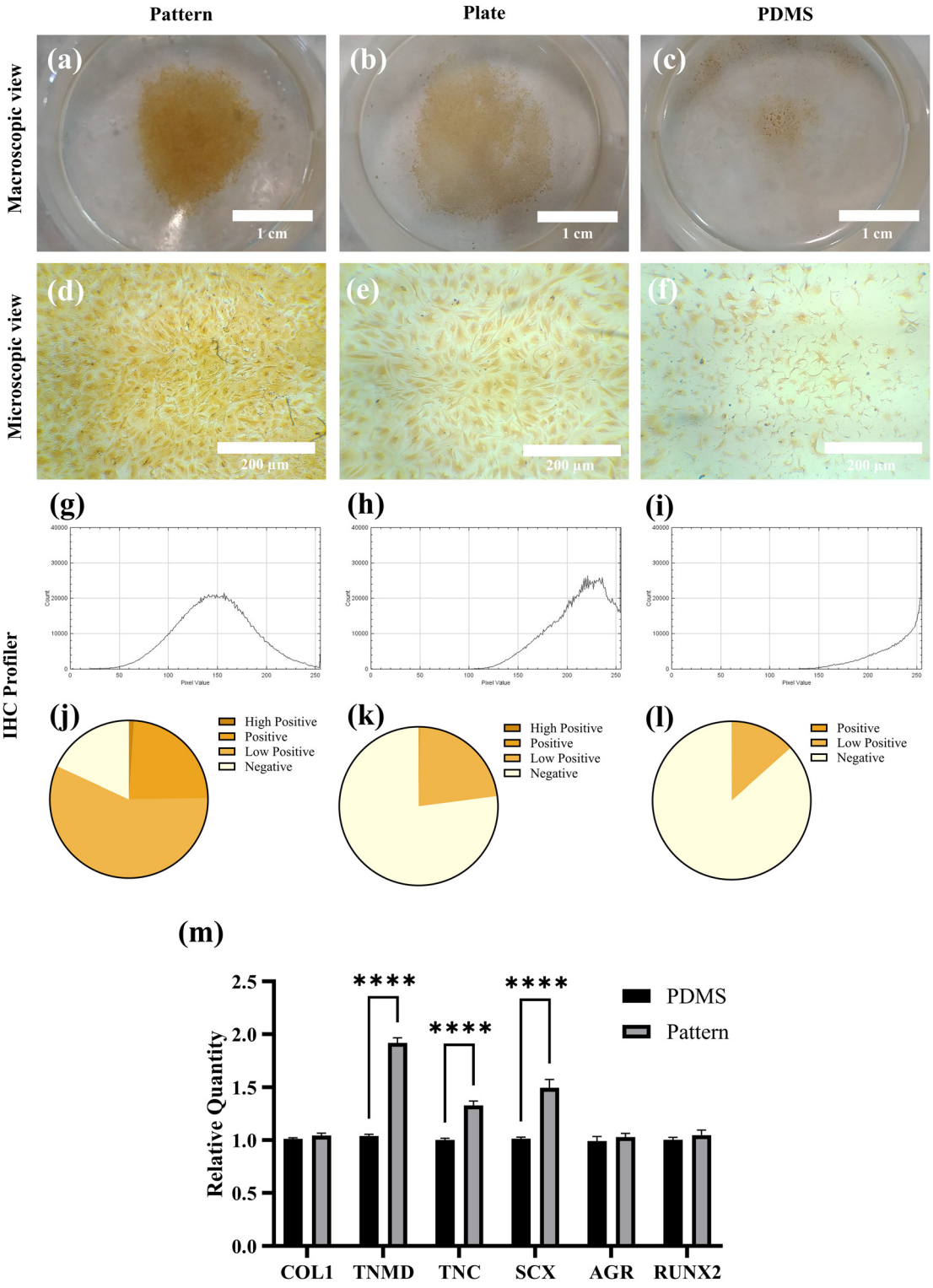

Fig. 3 *In vitro* evaluation of the imprint differentiation method. Anti-tenomodulin staining results of ADSCs after culturing on imprinted substrates (Pattern) (a, d, g and j), normal TCP culture plate (Plate) (b, e, h and k), and PDMS without a pattern (PDMS) (c, f, i and l). (j) presents a positive result based on the IHC profiler report. (k) and (l) present the negative results based on the IHC profiler report (n = 5). Real-time PCR. The graph in (m) shows the expression profiling of collagen type 1 (COL1), tenomodulin (TNMD), tenascin (TNC), SCX, AGR, and RUNX2 genes (n = 4).

tance between sutures was 3.64 times greater in length compared to other groups (Fig. 4B3). In other groups that received the scaffold, regardless of being cell-seeded, the tendon could preserve its length (Fig. 4B1 and B2). From these results, it can be inferred that applying the scaffold could help preserve the tendon length in tendon defects. Other studies also support

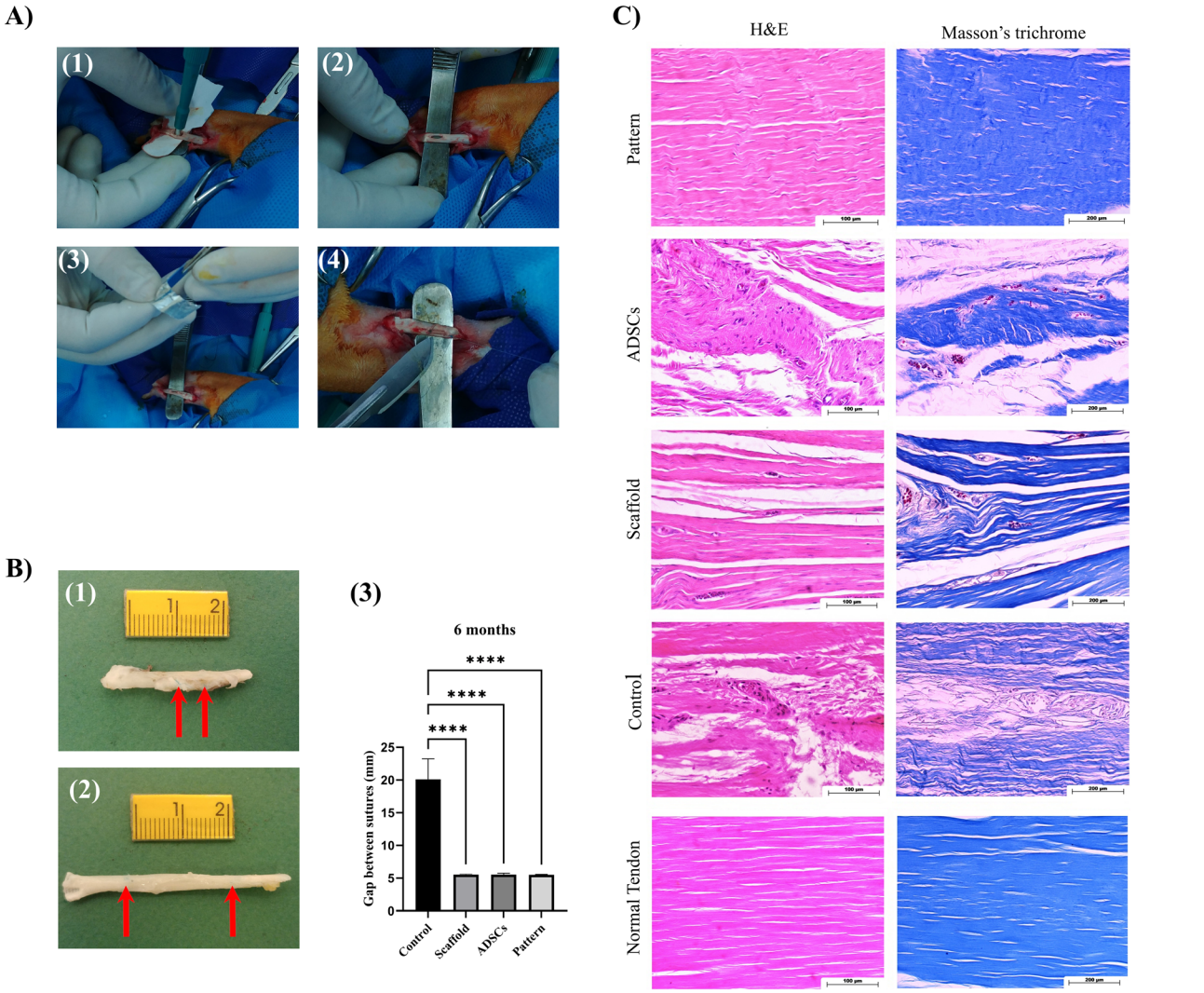

Fig. 4 Surgery steps (A) and post-treatment macroscopic (B) and microscopic (C) observations. The defect-forming process of a rabbit gastrocnemius tendon followed by an autograft induction is presented in (A1–A4). A comparison between the wound area length in the study group treated with the differentiated ADSC-seeded scaffold and the one left untreated is presented in (B1 and B2), respectively. Arrows denote the indicators of defect margins (sutures). This figure compares the length of the wound area (gap between sutures) after 24 weeks in the study groups (B3). (C) shows microscopy images of H&E and Masson's trichrome staining of fixed, longitudinal sections of tendon tissues. Well-organized parallelly aligned collagen fibers in the Pattern group are more similar to those in the normal tendon. Vascularization and irregularity of collagen fibers in the ADSC group and thick, well-aligned collagen fibers in the Scaffold group are remarkable in these figures.

the finding that the tendon length increases after an injury. Maquirriain *et al.* considered an Achilles tendon defect as an example of the most therapeutically challenging injury.[62] They concluded that clinical approaches aiming to manage tendon defects should focus mainly on maintaining the natural tendon length and preserving its resistance. Therefore, conserving natural tendon length is the desired achievement of the present research.

Histopathological analysis. A histopathological analysis with semiquantitative scoring was conducted to evaluate the effects of the scaffold and imprint differentiation method. After 24 weeks of treatment, fixed longitudinal histological specimens were stained with H&E and Masson's trichrome dyes (Fig. 4C). The histological scoring system developed by Stoll *et al.* evaluates tissue samples according to various histological features.[56] This system categorizes histological findings into scores based on histological specimens, which reflect the extent of tissue changes, providing a structured approach to assess tissue regeneration. The specifics of these scores are outlined in ESI Table 2† for a clear interpretation. GraphPad Prism 9.0.0 for Windows software was employed for statistical analysis. The statistical analysis was performed on the total score and each specific histological index. Fig. 5 visualizes the statistical analysis of the scoring. Data were depicted as mean and standard deviation. The comparison was performed by one-way ANOVA with the Bonferroni test.

The most important result of this study is the total score graph (Fig. 5a). The Pattern group shows significantly better

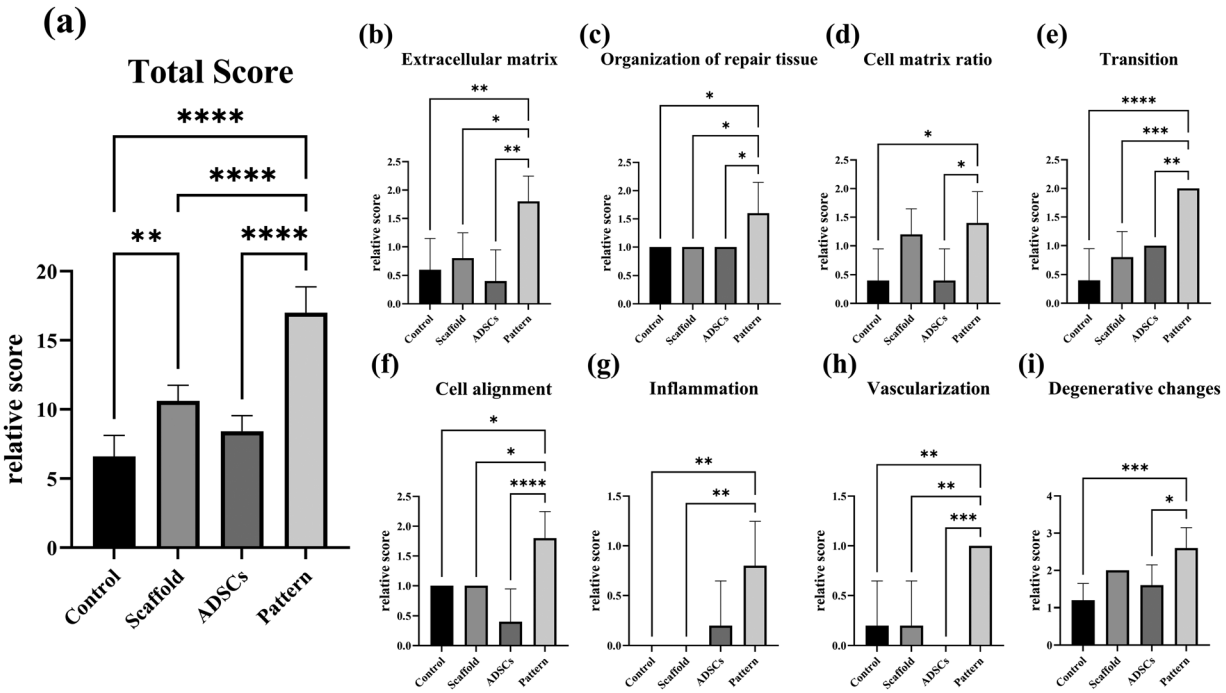

Fig. 5 Statistical analysis based on the semiquantitative scoring of histological indexes and the total histological scores. Total score (a), extracellular matrix (b), organization of repaired tissue (c), cell–matrix ratio (d), transition from defective to normal tissue (e), cell alignment (f), inflammation (g), vascularization in the defect area (h), and degenerative changes/tissue metaplasia (i) (*$p < 0.05$, **$p < 0.01$, ***$p < 0.001$, and ****$p < 0.0001$).

attributes than all other groups. Interestingly, the scaffold group showed a significant improvement compared to the control group, indicating the positive effects of applying collagen-coated PCL parallel fibers and the synergic effect of the imprint differentiation method. Surprisingly, the Scaffold group showed a higher average than the ADSC group. However, this difference was not statistically significant.

The healing tissue in the Pattern group, which had the highest average total histological scores, mimicked the typical tendon tissue microstructure and displayed well-organized, wavy, parallel collagen fibers and elongated nucleus cells resembling tenocytes. In a longitudinal section of the normal rabbit tendon tissue, we observed densely packed, highly parallel collagen fibers with a few tenocytes expanded between the fibers.[63] However, in our study, the cell/matrix ratio of the Pattern group in most areas where healing occurred was slightly higher than the normal physiological cellularity of tendon tissue. Apart from some giant cells around the scaffold residues, as in other study groups, no vascular structures or inflammatory cell infiltrations were detected in the Pattern group (Fig. 4C). In five out of twelve indexes, we observed significant differences in favor of the Pattern group compared to all other groups. These five indexes were the ECM, organization of repaired tissue, the transition from defective to normal tissue, cell alignment, and vascularization in the defect area (Fig. 5b, c, e, f and h, respectively). The Pattern group exhibited significant differences across all indexes compared to the control group, reflected in a significantly higher total score than those of all other groups.

An area of the injured tendon tissue of the Pattern group mimicked the typical tendon tissue microstructure. Well-organized wavy parallel collagen fibers with elongated nucleus tenocyte-like cells were among the favorable features of this treatment outcome. Owing to the differentiated ADSCs, tissue regeneration was significantly enhanced compared to that of other groups.

Interestingly, the Scaffold group was not significantly different from the Pattern group in the cell–matrix ratio and degenerative changes (Fig. 5d and i), indicating the positive effect of using collagen-coated parallel fibers. This index comparison may not show a significant difference between the scaffold group and the other two groups; however, it reflects the difference in the total score comparison. Twenty-four weeks after scaffold (with or without cells) implantation to the injured tendon, it did not absorb completely, and the remnant scaffold was visible in some areas within the histological sections. Thus, the scaffold group got no score in the inflammation index, exacerbated by the giant cell and mononuclear inflammatory cells surrounding the scaffold remnant (ESI Fig. 3†). The use of bovine collagen could be responsible for the observed reaction, given that the mismatched source of collagen could influence immune responses. We noticed that adding cells to the scaffold could reduce inflammation, as seen in Fig. 5g. Although the Scaffold group was not accompanied by cells, the neighboring cells and migration of other cells would compensate to some extent. Other studies, like that of Smith *et al.*, have reported that the rise in cellular population and tissue expansion following an injury is due to

the activity of resident cells within the tissue or stem cells that migrate to the injured area.[64] It can be concluded that the scaffold structure successfully attracts and supports more competent cells to the defect area than the control group. To some extent, these migrated and neighboring cells outperform the nondifferentiated ADSCs.

The average score of the undifferentiated ADSC-seeded scaffold (ADSC group) did not show a positive effect on the regeneration process compared to the Scaffold group. It even unfavorably affected the wounded area in the ECM, cell alignment, and vascularization indexes (not statistically significant). A study by Moradi *et al.* found that the regeneration capacity of ADSCs was negligible when they were not differentiated.[65] This means that sufficient cues need to be provided for stem cells *in vitro* before transplantation. Therefore, promoting the differentiation of ADSCs before implanting them into the body is the key to yielding desirable outcomes regarding tissue regeneration. In the ADSC study group, transformed wound tissue with an irregularity of collagen fibers and (mainly) the distinct presence of cells with round nuclei and high vascularization was observed. Likewise, the control study groups exhibited irregular collagen fibers with disorganized cellular distribution and alignment.

The study duration plays an imperative role in the judgment of treatment outcomes in tendon tissue, and some indexes, such as vascularization, could be interpreted differently depending on the healing stage. Vascularization serves as an effective mechanism for tissue regeneration; however, if it extends over 24 weeks, it interprets negatively in tendon tissue regeneration. Caplan *et al.* concluded that ADSCs act as signaling cells, contributing therapeutically *via* signal transduction.[66] This cell signaling within an injured tissue acts as a double-edged sword. Stem cell signaling is believed to keep the injured site dynamics by constantly generating blood vessels to meet the needs of the injured tissue. Nevertheless, existing blood vessels in tendon tissue are interpreted negatively in repaired tendon tissue. Several studies conducted in this field had a shorter evaluation span between 6 and 8 weeks.[67] This may explain why they reported the positive effect of using undifferentiated ADSCs. However, the present study firmly rejects the speculation of employing ADSCs to magnify regeneration in long-term treatment. More importantly, the present study identified that inducing ADSC differentiation by tailoring the cell culture substrate to recapitulate the tenocyte niche significantly improved tendon regeneration. Nonetheless, the data acquired from this study do not identify stem cell signaling transduction as a supportive mechanism for regeneration over 24 weeks.

We performed mechanical tests on the treated groups to gain some perspective for future studies (ESI Fig. 4†). The control and ADSC groups showed the lowest tensile strength in the mechanical tests. We did not observe distinctive differences between the Scaffold and Pattern groups. Interestingly, the Scaffold group showed superior results compared to the ADSC group, which is consistent with the histopathology results.

Although we were unable to evaluate every possible aspect of this study, regarding the current results, we can suggest that the differentiation of ADSCs by the imprinting technique is a safe, simple, and powerful way. We strongly advocate using scaffolds that further mimic the host tissue structure. Moreover, we suggest using collagen sourced from the same species to avoid unnecessary immune responses. Further studies need to be conducted to find the exact mechanism of the effectiveness of PDMS imprinting. Additionally, we suggest using other larger animal models to confirm the safety and competency of the presented tendon graft further.

Conclusions

This study proves the efficiency of tenocyte-imprinted substrates in inducing tenogenic signals in ADSCs and designed scaffolds to aid tendon regeneration. Tendon reconstruction in a rabbit model after transplantation of seeded differentiated ADSCs in the injured sites was evaluated. In addition, tenogenic differentiation was induced in ADSCs by tenocyte-imprinted substrates. Statistical analysis of total histological scores showed significant differences between the results obtained from the groups treated with the scaffold seeded with differentiated ADSCs (Pattern) and all the other groups. The results also indicate that nondifferentiated ADSCs do not contribute to tendon reconstruction.

Conflicts of interest

The authors declare that they have no known conflict of interest or personal relationships that could have appeared to influence the work reported in this paper.

Data availability

All data generated or analyzed during this study are available from the corresponding author, Shahin Bonakdar (shahinbonakdar@yahoo.com), upon reasonable request.

Acknowledgements

This research was supported by the Elite Researcher Grant Committee under the award number 971310 from the National Institute for Medical Research Development (NIMAD).

References

1 V. Citro, M. Clerici, A. R. Boccaccini, G. D. Porta, N. Maffulli and N. R. Forsyth, Tendon tissue engineering: An overview of biologics to promote tendon healing and repair, *J. Tissue Eng.*, 2023, **14**, 20417314231196275, DOI: 10.1177/20417314231196275.

2 D. Docheva, S. A. Müller, M. Majewski and C. H. Evans, Biologics for tendon repair, *Adv. Drug Delivery Rev.*, 2015, **84**, 222–239, DOI: 10.1016/j.addr.2014.11.015.
3 N. A. Dyment and J. L. Galloway, Regenerative Biology of Tendon: Mechanisms for Renewal and Repair, *Curr. Mol. Biol. Rep.*, 2015, **1**, 124–131, DOI: 10.1007/s40610-015-0021-3.
4 S. Chen, J. Wang, Y. Chen, X. Mo and C. Fan, Tenogenic adipose-derived stem cell sheets with nanoyarn scaffolds for tendon regeneration, *Mater. Sci. Eng., C*, 2021, **119**, 111506, DOI: 10.1016/j.msec.2020.111506.
5 B. Bellei, E. Migliano, M. Tedesco, S. Caputo, F. Papaccio, G. Lopez and M. Picardo, Adipose tissue-derived extracellular fraction characterization: Biological and clinical considerations in regenerative medicine, *Stem Cell Res. Ther.*, 2018, **9**, 1–18, DOI: 10.1186/s13287-018-0956-4.
6 S. K. Kureel, P. Mogha, A. Khadpekar, V. Kumar, R. Joshi, S. Das, J. Bellare and A. Majumder, Soft substrate maintains proliferative and adipogenic differentiation potential of human mesenchymal stem cells on long-term expansion by delaying senescence, *Biol. Open*, 2019, **8**, bio039453, DOI: 10.1242/bio.039453.
7 P. Ke, X. N. Jiao, X. H. Ge, W. M. Xiao and B. Yu, From macro to micro: Structural biomimetic materials by electrospinning, *RSC Adv.*, 2014, **4**, 39704–39724, DOI: 10.1039/c4ra05098c.
8 S. Mohammadi, S. Ramakrishna, S. Laurent, M. A. Shokrgozar, D. Semnani, D. Sadeghi, S. Bonakdar and M. Akbari, Fabrication of Nanofibrous PVA/Alginate-Sulfate Substrates for Growth Factor Delivery, *J. Biomed. Mater. Res., Part A*, 2019, **107**, 403–413, DOI: 10.1002/jbm.a.36552.
9 S. Wu, J. Liu, Y. Qi, J. Cai, J. Zhao, B. Duan and S. Chen, Tendon-bioinspired wavy nanofibrous scaffolds provide tunable anisotropy and promote tenogenesis for tendon tissue engineering, *Mater. Sci. Eng., C*, 2021, **126**, 112181, DOI: 10.1016/j.msec.2021.112181.
10 Y. Panahi-Joo, A. Karkhaneh, A. Nourinia, B. Abd-Emami, B. Negahdari, P. Renaud and S. Bonakdar, Design and fabrication of a nanofibrous polycaprolactone tubular nerve guide for peripheral nerve tissue engineering using a two-pole electrospinning system, *Biomed. Mater.*, 2016, **11**, 25017.
11 J. Xue, T. Wu, Y. Dai and Y. Xia, Electrospinning and electrospun nanofibers: Methods, materials, and applications, *Chem. Rev.*, 2019, **119**, 5298–5415, DOI: 10.1021/acs.chemrev.8b00593.
12 Y. Habibi, A. L. Goffin, N. Schiltz, E. Duquesne, P. Dubois and A. Dufresne, Bionanocomposites based on poly(ε-caprolactone)-grafted cellulose nanocrystals by ring-opening polymerization, *J. Mater. Chem.*, 2008, **18**, 5002–5010, DOI: 10.1039/b809212e.
13 T. Lim, J. Yoon, C. Lee, K. Y. Baek, J. W. Jeon and S. Cho, Self-Healable and Degradable Polycaprolactone-Based Polymeric Binders for Lithium-Ion Batteries, *ACS Appl. Polym. Mater.*, 2024, **6**, 4050–4059, DOI: 10.1021/acsapm.4c00097.
14 Y. Zhu, C. Gao, X. Liu and J. Shen, Surface Modification of Polycaprolactone Membrane via Aminolysis and Biomacromolecule Immobilization for Promoting Cytocompatibility of Human Endothelial Cells, *Biomacromolecules*, 2002, **3**, 1312–1319, DOI: 10.1021/bm020074y.
15 M. Khatri, R. J. Naughton, T. Clifford, L. D. Harper and L. Corr, The effects of collagen peptide supplementation on body composition, collagen synthesis, and recovery from joint injury and exercise: a systematic review, *Amino Acids*, 2021, **53**, 1493–1506, DOI: 10.1007/s00726-021-03072-x.
16 P. P. S. S. Abadi, J. C. Garbern, S. Behzadi, M. J. Hill, J. S. Tresback, T. Heydari, M. R. Ejtehadi, N. Ahmed, E. Copley, H. Aghaverdi, R. T. Lee, O. C. Farokhzad and M. Mahmoudi, Engineering of Mature Human Induced Pluripotent Stem Cell-Derived Cardiomyocytes Using Substrates with Multiscale Topography, *Adv. Funct. Mater.*, 2018, **28**, 1707378, DOI: 10.1002/adfm.201707378.
17 G. Abagnale, A. Sechi, M. Steger, Q. Zhou, C. C. Kuo, G. Aydin, C. Schalla, G. Müller-Newen, M. Zenke, I. G. Costa, P. van Rijn, A. Gillner and W. Wagner, Surface Topography Guides Morphology and Spatial Patterning of Induced Pluripotent Stem Cell Colonies, *Stem Cell Rep.*, 2017, **9**, 654–666, DOI: 10.1016/j.stemcr.2017.06.016.
18 M. Ali and J. B. Shear, Real time remodeling of cellular morphology using optical imprinting of cell-culture substrates, *Biomed. Phys. Eng. Express*, 2019, **5**, 035029.
19 E. Costa, C. González-García, J. L. Gómez Ribelles and M. Salmerón-Sánchez, Maintenance of chondrocyte phenotype during expansion on PLLA microtopographies, *J. Tissue Eng.*, 2018, **9**, 2041731418789829, DOI: 10.1177/2041731418789829.
20 B. Liu, C. Tao, Z. Wu, H. Yao and D. A. Wang, Engineering strategies to achieve efficient in vitro expansion of haematopoietic stem cells: development and improvement, *J. Mater. Chem. B*, 2022, **10**, 1734–1753, DOI: 10.1039/d1tb02706a.
21 J. O. Abaricia, N. Farzad, T. J. Heath, J. Simmons, L. Morandini and R. Olivares-Navarrete, Control of innate immune response by biomaterial surface topography, energy, and stiffness, *Acta Biomater.*, 2021, **133**, 58–73, DOI: 10.1016/j.actbio.2021.04.021.
22 F. Han, C. Zhu, Q. Guo, H. Yang and B. Li, Cellular modulation by the elasticity of biomaterials, *J. Mater. Chem. B*, 2016, **4**, 9–26, DOI: 10.1039/c5tb02077h.
23 K. Kamguyan, S. Z. Moghaddam, A. Nazbar, S. M. A. Haramshahi, S. Taheri, S. Bonakdar and E. Thormann, Cell-imprinted substrates: In search of nano-topographical fingerprints that guide stem cell differentiation, *Nanoscale Adv.*, 2021, **3**, 333–338, DOI: 10.1039/d0na00692k.
24 C. Y. Yang, W. Y. Huang, L. H. Chen, N. W. Liang, H. C. Wang, J. Lu, X. Wang and T. W. Wang, Neural tissue engineering: The influence of scaffold surface topography and extracellular matrix microenvironment, *J. Mater. Chem. B*, 2021, **9**, 567–584, DOI: 10.1039/d0tb01605e.

25 E. S. Place, N. D. Evans and M. M. Stevens, Complexity in biomaterials for tissue engineering, *Nat. Mater.*, 2009, **8**, 457–470, DOI: 10.1038/nmat2441.
26 S. M. A. Haramshahi, S. Bonakdar, M. Moghtadaei, K. Kamguyan, E. Thormann, S. Tanbakooei, S. Simorgh, P. Brouki-Milan, N. Amini and N. Latifi, Tenocyte-imprinted substrate: A topography-based inducer for tenogenic differentiation in adipose tissue-derived mesenchymal stem cells, *Biomed. Mater.*, 2020, **15**, 035014.
27 S. Bonakdar, M. Mahmoudi, L. Montazeri, M. Taghipoor, A. Bertsch, M. A. Shokrgozar, S. Sharifi, M. Majidi, O. Mashinchian, M. Hamrang Sekachaei, P. Zolfaghari and P. Renaud, Cell-Imprinted Substrates Modulate Differentiation, Redifferentiation, and Transdifferentiation, *ACS Appl. Mater. Interfaces*, 2016, **8**, 13777–13784, DOI: 10.1021/acsami.6b03302.
28 K. Kamguyan, A. A. Katbab, M. Mahmoudi, E. Thormann, S. Zajforoushan Moghaddam, L. Moradi and S. Bonakdar, An engineered cell-imprinted substrate directs osteogenic differentiation in stem cells, *Biomater. Sci.*, 2018, **6**, 189–199, DOI: 10.1039/c7bm00733g.
29 Z. S. Ghazali, M. Eskandari, S. Bonakdar, P. Renaud, O. Mashinchian, S. Shalileh, F. Bonini, I. Uckay, O. Preynat-Seauve and T. Braschler, Neural priming of adipose-derived stem cells by cell-imprinted substrates, *Biofabrication*, 2021, **13**, DOI: 10.1088/1758-5090/abc66f.
30 O. Mashinchian, S. Bonakdar, H. Taghinejad, V. Satarifard, M. Heidari, M. Majidi, S. Sharifi, A. Peirovi, S. Saffar, M. Taghinejad, M. Abdolahad, S. Mohajerzadeh, M. A. Shokrgozar, S. M. Rezayat, M. R. Ejtehadi, M. J. Dalby and M. Mahmoudi, Cell-imprinted substrates act as an artificial niche for skin regeneration, *ACS Appl. Mater. Interfaces*, 2014, **6**, 13280–13292, DOI: 10.1021/am503045b.
31 N. Jung, S. Park, Y. Choi, J.-W. Park, Y. Hong, H. Park, Y. Yu, G. Kwak, H. Kim and K.-H. Ryu, Tonsil-derived mesenchymal stem cells differentiate into a Schwann cell phenotype and promote peripheral nerve regeneration, *Int. J. Mol. Sci.*, 2016, **17**, 1867.
32 E. A. Lee, S. G. Im and N. S. Hwang, Efficient myogenic commitment of human mesenchymal stem cells on biomimetic materials replicating myoblast topography, *Biotechnol. J.*, 2014, **9**, 1604–1612, DOI: 10.1002/biot.201400020.
33 S. Yazdian Kashani, M. Keshavarz Moraveji, M. Taghipoor, R. Kowsari-Esfahan, A. A. Hosseini, L. Montazeri, M. M. Dehghan, H. Gholami, S. Farzad-Mohajeri, M. Mehrjoo, M. Majidi, P. Renaud and S. Bonakdar, An integrated microfluidic device for stem cell differentiation based on cell-imprinted substrate designed for cartilage regeneration in a rabbit model, *Mater. Sci. Eng., C*, 2021, **121**, 111794, DOI: 10.1016/j.msec.2020.111794.
34 A. Nazbar, S. Samani, S. Yazdian Kashani, A. Amanzadeh, S. Shoeibi and S. Bonakdar, Molecular imprinting as a simple way for the long-term maintenance of the stemness and proliferation potential of adipose-derived stem cells: an in vitro study, *J. Mater. Chem. B*, 2022, **10**, 6816–6830, DOI: 10.1039/d2tb00279e.
35 S. Taheri, Z. S. Ghazali, L. Montazeri, F. A. Ebrahim, J. Javadpour, K. Kamguyan, E. Thormann, P. Renaud and S. Bonakdar, Engineered substrates incapable of induction of chondrogenic differentiation compared to the chondrocyte imprinted substrates, *Biomed. Mater.*, 2023, **18**, 025006.
36 S. Yazdian Kashani, A. Afzalian, F. Shirinichi and M. K. Moraveji, Microfluidics for core-shell drug carrier particles - a review, *RSC Adv.*, 2020, **11**, 229–249, DOI: 10.1039/d0ra08607j.
37 F. Etezadi, M. N. T. Le, H. Shahsavarani, A. Alipour, N. Moazzezy, S. Samani, A. Amanzadeh, S. Pahlavan, S. Bonakdar, M. A. Shokrgozar and K. Hasegawa, Optimization of a PDMS-Based Cell Culture Substrate for High-Density Human-Induced Pluripotent Stem Cell Adhesion and Long-Term Differentiation into Cardiomyocytes under a Xeno-Free Condition, *ACS Biomater. Sci. Eng.*, 2022, **8**, 2040–2052, DOI: 10.1021/acsbiomaterials.2c00162.
38 M. Ehrbar, S. C. Rizzi, R. Hlushchuk, V. Djonov, A. H. Zisch, J. A. Hubbell, F. E. Weber and M. P. Lutolf, Enzymatic formation of modular cell-instructive fibrin analogs for tissue engineering, *Biomaterials*, 2007, **28**, 3856–3866, DOI: 10.1016/j.biomaterials.2007.03.027.
39 R. C. Lyon, F. Zanella, J. H. Omens and F. Sheikh, Mechanotransduction in cardiac hypertrophy and failure, *Circ. Res.*, 2015, **116**, 1462–1476, DOI: 10.1161/CIRCRESAHA.116.304937.
40 Y. Shao, J. M. Mann, W. Chen and J. Fu, Global architecture of the F-actin cytoskeleton regulates cell shape-dependent endothelial mechanotransduction, *Integr. Biol.*, 2014, **6**, 300–311, DOI: 10.1039/c3ib40223a.
41 H. Kavand, H. Van Lintel, S. Bakhshi Sichani, S. Bonakdar, H. Kavand, J. Koohsorkhi and P. Renaud, Cell-Imprint Surface Modification by Contact Photolithography-Based Approaches: Direct-Cell Photolithography and Optical Soft Lithography Using PDMS Cell Imprints, *ACS Appl. Mater. Interfaces*, 2019, **11**, 10559–10566, DOI: 10.1021/acsami.9b00523.
42 O. Mashinchian, S. Bonakdar, H. Taghinejad, V. Satarifard, M. Heidari, M. Majidi, S. Sharifi, A. Peirovi, S. Saffar, M. Taghinejad, M. Abdolahad, S. Mohajerzadeh, M. A. Shokrgozar, S. M. Rezayat, M. R. Ejtehadi, M. J. Dalby and M. Mahmoudi, Cell-imprinted substrates act as an artificial niche for skin regeneration, *ACS Appl. Mater. Interfaces*, 2014, **6**, 13280–13292, DOI: 10.1021/am503045b.
43 M. Mahmoudi, S. Bonakdar, M. A. Shokrgozar, H. Aghaverdi, R. Hartmann, A. Pick, G. Witte and W. J. Parak, Cell-imprinted substrates direct the fate of stem cells, *ACS Nano*, 2013, **7**, 8379–8384, DOI: 10.1021/nn403844q.
44 C. Zhang, X. Wang, E. Zhang, L. Yang, H. Yuan, W. Tu, H. Zhang, Z. Yin, W. Shen, X. Chen, Y. Zhang and H. Ouyang, An epigenetic bioactive composite scaffold with well-aligned nanofibers for functional tendon tissue engineering, *Acta Biomater.*, 2018, **66**, 141–156, DOI: 10.1016/j.actbio.2017.09.036.
45 Y. Panahi-Joo, A. Karkhaneh, A. Nourinia, B. Abd-Emami, B. Negahdari, P. Renaud and S. Bonakdar, Design and fab-

rication of a nanofibrous polycaprolactone tubular nerve guide for peripheral nerve tissue engineering using a two-pole electrospinning system, *Biomed. Mater.*, 2016, **11**, 25017.

46 L. C. U. Junqueira, G. Bignolas and R. R. Brentani, *Picrosirius staining plus polarization microscopy, a specific method for collagen detection in tissue sections*, 1979.

47 J. A. Kiernan, Sirius Red for Collagen Staining Protocol, n. d. **https://www.histosearch.com**.

48 S. Sivakumar, V. Sadaiyandi, S. Swaminathan and R. Ramalingam, Biocompatibility, anti-hemolytic, and antibacterial assessments of electrospun PCL/collagen composite nanofibers loaded with Acanthophora spicifera extracts mediated copper oxide nanoparticles, *Biocatal. Agric. Biotechnol.*, 2024, **55**, 102983, DOI: **10.1016/j.bcab.2023.102983**.

49 S. R. Chowdhury, G. Mondal, P. Ratnayake and B. Basu, Three-Dimensional Extrusion Printed Urinary Specific Grafts: Mechanistic Insights into Buildability and Biophysical Properties, *ACS Biomater. Sci. Eng.*, 2024, **10**, 1040–1061, DOI: **10.1021/acsbiomaterials.3c01422**.

50 K. Sakthiabirami, J. H. Kang, J. G. Jang, V. Soundharrajan, H. P. Lim, K. D. Yun, C. Park, B. N. Lee, Y. P. Yang and S. W. Park, Hybrid porous zirconia scaffolds fabricated using additive manufacturing for bone tissue engineering applications, *Mater. Sci. Eng., C*, 2021, **123**, 111950, DOI: **10.1016/j.msec.2021.111950**.

51 S. L. Leary, American Veterinary Medical Association, AVMA guidelines for the euthanasia of animals: 2020 edition, n.d.

52 Y. Cao, J. Yan, Z. Dong, J. Wang, X. Jiang, T. Cui, Y. Huang and H. Liu, Adipose-derived Mesenchymal Stem Cells are Ideal for the Cell-based Treatment of Refractory Wounds: Strong Potential for Angiogenesis, *Stem Cell Rev. Rep.*, 2024, **20**, 313–328, DOI: **10.1007/s12015-023-10641-y**.

53 G. Zhang, Y. Ezura, I. Chervoneva, P. S. Robinson, D. P. Beason, E. T. Carine, L. J. Soslowsky, R. v. Iozzo and D. E. Birk, Decorin regulates assembly of collagen fibrils and acquisition of biomechanical properties during tendon development, *J. Cell. Biochem.*, 2006, **98**, 1436–1449, DOI: **10.1002/jcb.20776**.

54 H. Tavassoli, J. Javadpour, M. Taheri, M. Mehrjou, N. Koushki, F. Arianpour, M. Majidi, J. Izadi-Mobarakeh, B. Negahdari, P. Chan, M. E. Warkiani and S. Bonakdar, Incorporation of Nanoalumina Improves Mechanical Properties and Osteogenesis of Hydroxyapatite Bioceramics, *ACS Biomater. Sci. Eng.*, 2018, **4**, 1324–1336, DOI: **10.1021/acsbiomaterials.7b00754**.

55 F. Varghese, A. B. Bukhari, R. Malhotra and A. De, IHC profiler: An open source plugin for the quantitative evaluation and automated scoring of immunohistochemistry images of human tissue samples, *PLoS One*, 2014, **9**, e96801, DOI: **10.1371/journal.pone.0096801**.

56 C. Stoll, T. John, C. Conrad, A. Lohan, S. Hondke, W. Ertel, C. Kaps, M. Endres, M. Sittinger, J. Ringe and G. Schulze-Tanzil, Healing parameters in a rabbit partial tendon defect following tenocyte/biomaterial implantation, *Biomaterials*, 2011, **32**, 4806–4815, DOI: **10.1016/j.biomaterials.2011.03.026**.

57 J. Peñaranda-Armbrecht, M. J. Correa-Quiceno, J. C. Caicedo-Angulo, P. A. Neuta-Arciniegas and J. Ó. Gutiérrez-Montes, Fabrication of multi-walled carbon nanotube/polycaprolactone scaffolds for possible application in tissue engineering, *J. Polym. Res.*, 2024, **31**, 64, DOI: **10.1007/s10965-024-03875-y**.

58 C. J. Cooper, A. K. Mohanty and M. Misra, Electrospinning process and structure relationship of biobased poly (butylene succinate) for nanoporous fibers, *ACS Omega*, 2018, **3**, 5547–5557.

59 J. Kastelic, A. Galeski and E. Baer, *The multicomposite structure of tendon*, Gordon and Breach Science Publishers Ltd, 1978.

60 M. Mozafari, S. Kargozar, G. T. de Santiago, M. R. Mohammadi, P. B. Milan, M. Foroutan Koudehi, B. Aghabarari and M. R. Nourani, Synthesis and characterisation of highly interconnected porous poly($ε$-caprolactone)-collagen scaffolds: a therapeutic design to facilitate tendon regeneration, *Mater. Technol.*, 2018, **33**, 29–37, DOI: **10.1080/10667857.2017.1379678**.

61 A. I. Gonçalves, P. M. Gershovich, M. T. Rodrigues, R. L. Reis and M. E. Gomes, Human adipose tissue-derived tenomodulin positive subpopulation of stem cells: A promising source of tendon progenitor cells, *J. Tissue Eng. Regener. Med.*, 2018, **12**, 762–774, DOI: **10.1002/term.2495**.

62 J. Maquirriain, Achilles tendon rupture: Avoiding tendon lengthening during surgical repair and rehabilitation, *Yale J. Biol. Med.*, 2011, **84**, 289–300.

63 M. Raspanti, T. Congiu and S. Guizzardi, Structural aspects of the extracellular matrix of the tendon: An atomic force and scanning electron microscopy study, *Arch. Histol. Cytol.*, 2002, **65**, 37–43, DOI: **10.1679/aohc.65.37**.

64 R. K. W. Smith, Stem cell technology in equine tendon and ligament injuries, *Vet. Rec.*, 2006, **158**, 140.

65 L. Moradi, M. Vasei, M. M. Dehghan, M. Majidi, S. Farzad Mohajeri and S. Bonakdar, Regeneration of meniscus tissue using adipose mesenchymal stem cells-chondrocytes co-culture on a hybrid scaffold: In vivo study, *Biomaterials*, 2017, **126**, 18–30, DOI: **10.1016/j.biomaterials.2017.02.022**.

66 A. I. Caplan, Mesenchymal stem cells: Time to change the name!, *Stem Cells Transl. Med.*, 2017, **6**, 1445–1451, DOI: **10.1002/sctm.17-0051**.

67 C. A. Uysal, M. Tobita, H. Hyakusoku and H. Mizuno, Adipose-derived stem cells enhance primary tendon repair: Biomechanical and immunohistochemical evaluation, *J. Plast., Reconstr. Aesthet. Surg.*, 2012, **65**, 1712–1719, DOI: **10.1016/j.bjps.2012.06.011**.